This article has been accepted for publication in a future issue of this journal, but has not been fully edited. Content may change prior to final publication. Citation information: DOI 10.1109/TNSRE.2014.2364618, IEEE Transactions on Neural Systems and Rehabilitation Engineering

Restoration of Gait for Spinal Cord Injury Patients using HAL with Intention Estimator for Preferable Swing Speed

Atsushi Tsukahara, Yasuhisa Hasegawa, Kiyoshi Eguchi, and Yoshiyuki Sankai

***Abstract*—This paper proposes a novel gait intention estimator for an exoskeleton-wearer who needs gait support owing to walking impairment. The gait intention estimator not only detects the intention related to the start of the swing leg based on the behavior of the center of ground reaction force (CoGRF), but also infers the swing speed depending on the walking velocity. The preliminary experiments categorized into two stages were performed on a mannequin equipped with the exoskeleton robot (Hybrid Assistive Limb: HAL) including the proposed estimator. The first experiment verified that the gait support system allowed the mannequin to walk properly and safely. In the second experiment, we confirmed the differences in gait characteristics attributed to the presence or absence of the proposed swing speed profile. As a feasibility study, we evaluated the walking capability of a severe spinal cord injury patient supported by the system during a 10-meter walk test. The results showed that the system enabled the patient to accomplish a symmetrical walk from both spatial and temporal standpoints while adjusting the speed of the swing leg. Furthermore, the critical differences of gait between our system and a knee-ankle-foot orthosis were obtained from the CoGRF distribution and the walking time. Through the tests, we demonstrated the effectiveness and practical feasibility of the gait support algorithms.**

***Index Terms*—Gait support, intention estimator, swing speed profile, exoskeleton robot, HAL.**

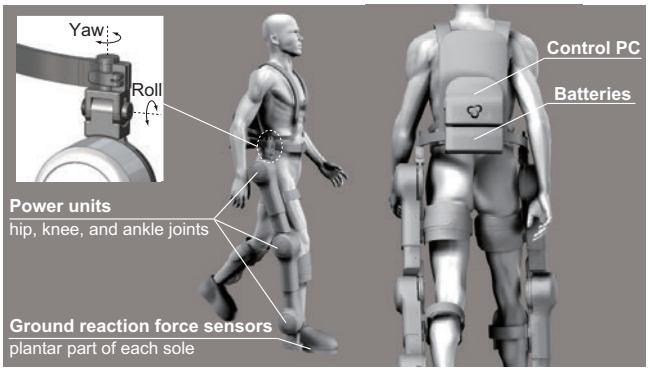

Fig. 1. System configurations of HAL for severe paraplegic patients who cannot stand up and walk by themselves. The HAL allows coordinated motion in the lower limbs around the pitch axis by adding an actuator to the ankle parts of the conventional HAL [10], [11]. In addition, the rotations of the hip joint around the roll and yaw axes are fixed at an arbitrary angle by each locking mechanism, and are also made as free as necessary. Also, a tri-axial accelerometer and a gyroscope are embedded into each link of HAL, and ground reaction force (GRF) sensors are installed in the plantar part of each sole. A computer and batteries are installed in the posterior region.

I. Introduction

SPINAL cord injury (SCI) patients who are forced to bedridden and wheelchair-bound are susceptible to developing decubitus, loss of bone density, articular contracture of the lower limbs, and deep-vein thrombosis (DVT) [1], [2]. If a blood clot formed by DVT breaks off from the vein wall in the lower limbs and then travels through the bloodstream to the pulmonary artery (PA), the patients are at a high risk of developing a pulmonary embolism (PE) resulting from the occlusion of the PA [3]. PE can be a cause of dyspnea or chest pain, which is a serious disease that has a more than 30% fatality rate [4], [5]. Gait support using an exoskeleton robot may be an effective way to address the above-mentioned problems because a patient wearing the robot moves their legs actively and the ground reaction force (GRF) stimulates the sensory and musculoskeletal system. Furthermore, the gait support has a particularly meaningful role in the regaining of walking function in severe SCI patients. It is therefore important that a robot can support the gait of complete as well as incomplete SCI patients and help them to maintain or regain their motor and sensory functions.

In our research project, the Hybrid Assistive Limb (HAL) has been developed to support the legged locomotion of paralyzed patients. The control system of HAL consists of a voluntary controller [6], [7] and an autonomous controller [8]–[11]. The voluntary controller assists the wearer's legged locomotion based on the bioelectrical signals (BES) that are generated just before the corresponding muscle contraction. However, it is difficult to apply this method to severely paralyzed patients who are unable to produce appropriate BES from the lower limbs. The autonomous control system, therefore, copes with the functional motion support of the patient without using the BES. Once the algorithm embedded into the control system infers the wearer's intention based on a preliminary motion, HAL autonomously starts the support of the desired motion. The preliminary motion is a kind of voluntary motion that is detectable immediately before a person starts the desired motion. In our previous work, HAL inferred the wearer's intention based on the beginning of the

A. Tsukahara is with Center for Cybernics Research, University of Tsukuba, 1-1-1, Tennodai, Tsukuba, Ibaraki, 305-8573, Japan (e-mail: tsukahara@ccr.tsukuba.ac.jp). Y. Hasegawa is with Department of Micro-Nano Systems Engineering Graduate School of Engineering, Nagoya University, Furocho, Chikusa-ku, Nagoya, Aichi, 464-8603, Japan. K. Eguchi is with Faculty of Medicine, University of Tsukuba, 1-1-1, Tennodai, Tsukuba, Ibaraki, 305-8575, Japan. Y. Sankai is with Faculty of Engineering, Information and Systems, University of Tsukuba, 1-1-1, Tennodai, Tsukuba, Ibaraki, 305-8573, Japan.

This article has been accepted for publication in a future issue of this journal, but has not been fully edited. Content may change prior to final publication. Citation information: DOI 10.1109/TNSRE.2014.2364618, IEEE Transactions on Neural Systems and Rehabilitation Engineering

leg-swing from the shift of the GRF, and supported the gait of a mild paraplegic patient who could stand up or walk slowly with canes [9]. After improving the algorithm and mechanical structure of HAL (see Fig. 1), the system detected the intention of complete SCI patients to start the desired motion and allowed them to stand up, sit down, and walk [10], [11].

Similarly, several studies have reported that a human-machine interface is essential for controlling an exoskeleton robot on the basis of the wearer's voluntary intention relevant to the initiation of the forward leg-swing [12]–[16]. Inputting commands via the wearer's voice [12] and the wristwatch style keypad [13] are used to switch the motional state. Other exoskeleton systems measure the upper arm and crutches motions [14] or the wheeled walker motion [15], [16] using inertial motion sensors and force sensors to detect the desired state from the wearer's more natural gestures while ensuring their safety. These papers point out the importance of transmitting the wearer's intention associated with voluntary motion to the exoskeleton robot so that the patient can intuitively start the desired motion. In the technology of exoskeleton robots mentioned above, the speed of the swing leg is always constant because the wearer's walk is controlled by one predesigned reference trajectory. As a result, the wearer might feel uncomfortable in regard to the constant speed of the swing leg depending on the degree of functional recovery in the lower limbs. If the swing speed provided by an exoskeleton robot varied based on the walking velocity, the wearer could swing the leg quickly to walk and to avoid stumbling. It is therefore quite important to adjust the swing leg at optimum speed during the gait support of an exoskeleton robot.

The purpose of this study is to propose a novel gait intention estimator that not only detects the moment that the swing leg starts, but also infers the swing speed so that the assistance of the system can synchronize the gait intention of a severe SCI patient at a higher level. Our experiments were conducted in three stages. First, we investigated the relationship between the speed of the swing leg and the duration of the double stance phase, measuring and analyzing the normal gait of a healthy participant on a treadmill with various belt speeds. Second, we performed preliminary experiments with a mannequin wearing HAL including the proposed algorithms before realistic tests with a severe SCI patient. The mannequin simulates the physical conditions of the lower limbs of a patient with completely impaired lower limb motor and sensory functions. Third, we performed realistic tests with a severe SCI patient for a practical feasibility evaluation of the proposed algorithms. The 10-meter walk test (10MWT) [17]–[19] and the spatial and temporal symmetries of the CoGRF were used to show how the algorithms helped the patient.

This paper is organized as follows. In Section II, we introduce the development of the gait support algorithms that consists of the gait intention estimator, the desired trajectory calculator, and the gait controller, based on the gait analysis of a healthy participant (see Fig. 2). Section III shows the preliminary experiments on gait support using the support system. Section IV presents the results of the realistic tests applied to the severe SCI patient. Sections V and VI are the discussion and the conclusions.

II. Methods

This section introduces the gait support algorithms: the gait intention estimator, the desired-trajectory calculator, and the controller, that improve the performance of the exoskeleton. The details and the relationships between them are described in the following subsections.

A. Gait intention estimator

1) Detection of gait intention: The measurement of BES is an established method used to detect the exoskeleton-wearer's intention related to the swing leg [6]–[8]. However, it is difficult to detect the required waveform amplitude to operate

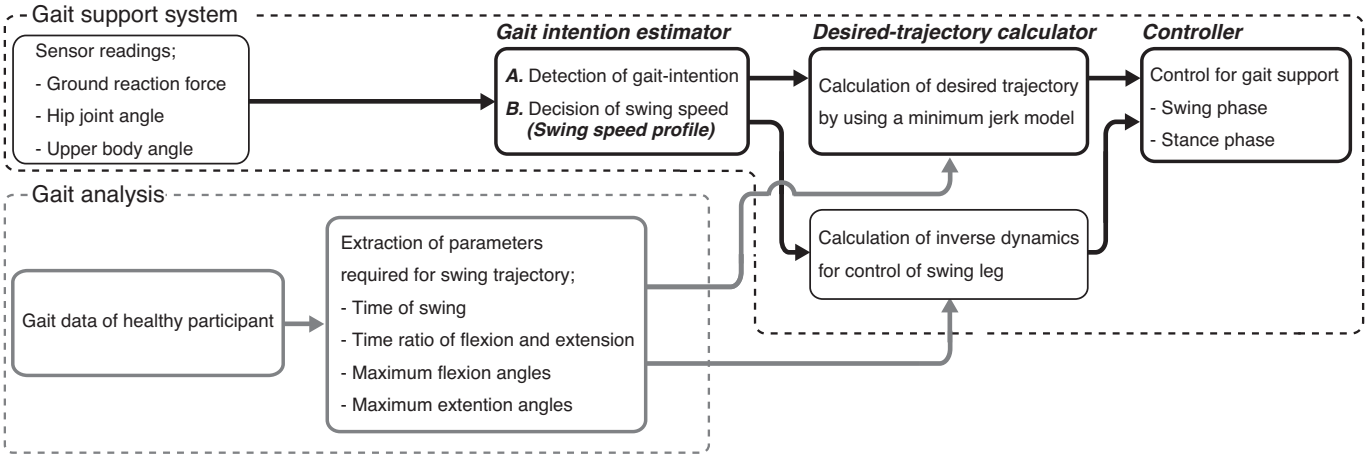

Fig. 2. Architecture of the gait support system. First, the gait intention estimator detects the exoskeleton (HAL) wearer's intention related to the beginning of the swing leg using the sensor readings, i.e., the ground reaction force, the hip joint angle, and the upper body angle during the double stance phase. The estimator also infers the swing speed based on a swing speed profile. Next, the system calculates the desired trajectories, which correspond to the speed of the swing leg determined by the estimator. The desired-trajectory calculator uses the parameters extracted from the gait analysis to calculate the trajectories corresponding to the walking velocity. At the same time, the system calculates the inverse dynamics based on the parameters corresponding to the estimated walking speed. Finally, the system controls the wearer's gait with the command torque from each power unit.

This article has been accepted for publication in a future issue of this journal, but has not been fully edited. Content may change prior to final publication. Citation information: DOI 10.1109/TNSRE.2014.2364618, IEEE Transactions on Neural Systems and Rehabilitation Engineering

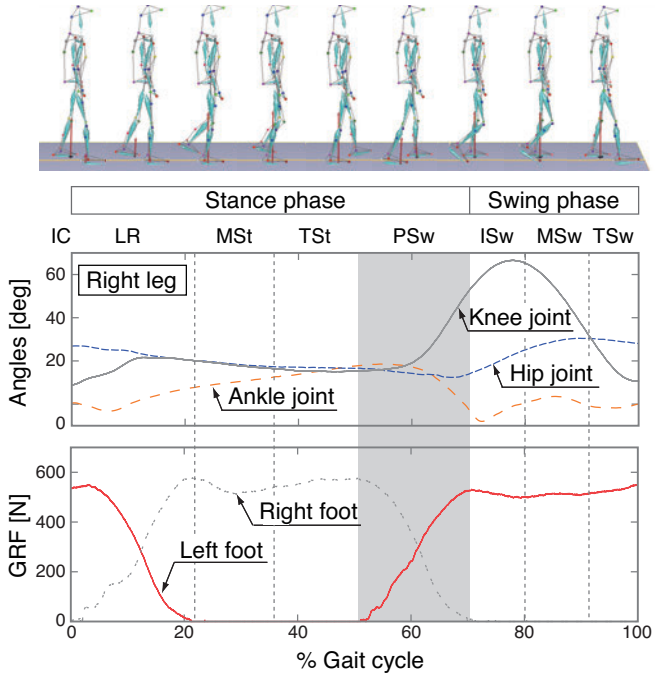

Fig. 3. Gait analysis of a healthy participant using a MAC3D system, which is a real-time optical motion capture (MotionAnalysis Inc.) and a treadmill-mounted force platform (Bertec Co.) during one gait cycle. Natural gait is classified into eight phases as follows: initial contact (IC), loading response (LR), mid stance (MSt), terminal stance (TSt), pre-swing (PSw), initial swing (ISw), mid swing (MSw), and terminal swing (TSw). The swing phase starts after the weight shift toward a previous swing leg side during the PSw.

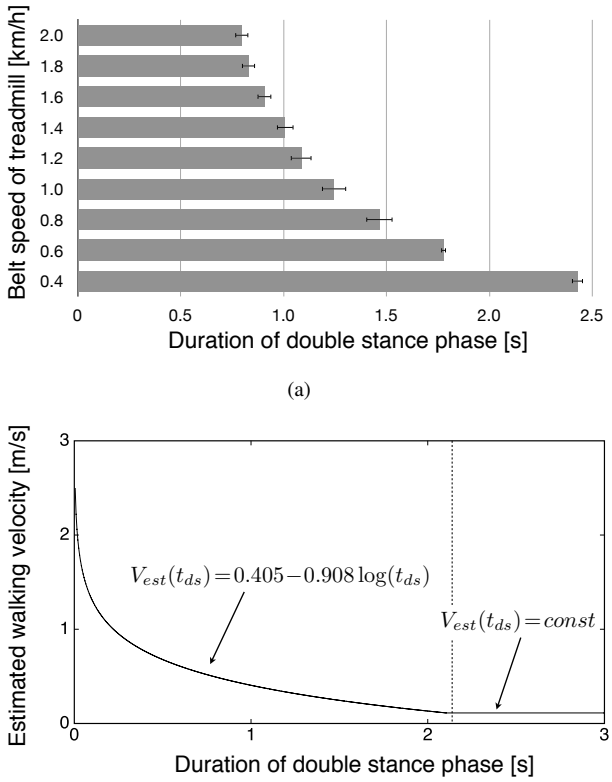

Fig. 4. (a) Relationship of the duration of the double stance phase vis-a-vis walking velocity during a healthy participant's gait. (b) Swing speed profile on the basis of the results of the gait analysis.

HAL properly from the severe SCI patient's legs. Thus, HAL needs to detect the wearer's intention based on a preliminary motion instead of detecting the BES. Humans always shift their weight to the next stance leg side before swinging the leg forward as shown in Fig. 3. This phenomenon is seen not only in healthy people but also in SCI patients who can partially move the CoGRF by inclining the body trunk. On the basis of the result shown in Fig. 3, this algorithm detects the exoskeleton-wearer's intention related to the start of the swing leg when the following inequalities are satisfied:

$$\begin{cases} f_f > f_b,\ \theta_{fh} \le \Theta_{fh},\ \text{and}\ |\phi_r| \ge \Phi_r, & (\text{if the step} = 1) \\ f_f > f_b\ \ \text{and}\ \ \theta_{fh} \le \Theta_{fh} & (\text{if the step} \ge 2) \end{cases} \quad (1)$$

where f_f, f_b, θ_{fh}, and ϕ_r are the GRF of the anterior and posterior legs, the hip joint angles of the anterior leg side, and the upper body angle around the roll axis, respectively. The constants Θ_{fh} and Φ_r, the thresholds for the start of the forward leg-swing, are determined from the results of the gait analysis of healthy people. Note that these constant values need to be adjusted slightly to fit the wearer's physical condition. When the system supports the standing position of the wearer, the upper body angle around the roll axis helps to distinguish the unintended deviation of center of gravity from the intention related to the swing leg. This algorithm, which does not use the BES, is a safe and effective method for detecting the severe SCI patient's intention related to the swing leg because he/she intuitively shifts their weight from the leg side to the opposite leg side by using a walking aid such as a walker or a cane.

2) Decision of swing speed: In our previous study, HAL with the gait intention estimator detected the patient's intention to start the swing leg based on the CoGRF behavior, and then the system controlled the coordinated motions of the wearer's leg using the constant desired trajectories [9], [11]. In the next stage, to provide the desired trajectories appropriate for the walking velocity, the estimator needs to infer the speed of the swing leg corresponding to the walking velocity as well as the moment to start the swing leg.

In general, the stance and swing periods in normal walking account for approximately 60% and 40% of one gait cycle (GC), respectively [20]. At the same time, the ratio of the double stance phase accounts for approximately 20% of the stance period. While the ratio of each period remains almost unchanged, the walking velocity increases inversely with the decrease of duration of the GC [21]. For this reason, the speed of the swing leg can be inferred by clarifying the relationship between the walking velocity and the duration of the double stance phase. Therefore, we analyzed the gait of a healthy participant to reveal the relationship mentioned above. The walking test was conducted on treadmill-mounted force plates so that the duration of the double stance phase could be measured at various belt speeds. From the results shown in Fig. 4a, we propose a swing speed profile that can

This article has been accepted for publication in a future issue of this journal, but has not been fully edited. Content may change prior to final publication. Citation information: DOI 10.1109/TNSRE.2014.2364618, IEEE Transactions on Neural Systems and Rehabilitation Engineering

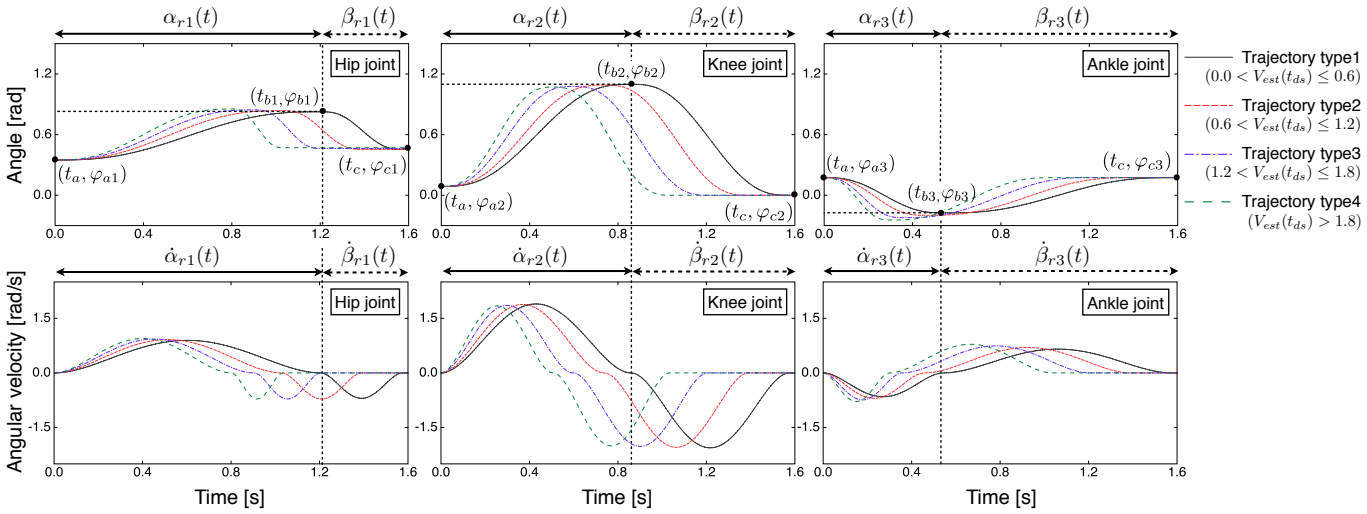

Fig. 5. Desired trajectory calculation for preferable swing speed. As a result of healthy participant's gait analysis, the trajectory of the swing leg proved to be classified with four main types according to the walking velocity between 0.4 km/h and 2.0 km/h. Therefore, we extracted the parameters (time of swing, time ratio of flexion and extension, maximum flexion angles, and maximum extension angles) from the gait analysis to calculate the desired trajectories corresponding to the walking velocity. The calculator selects the optimum parameters on the basis of the walking velocity $V_{est}(t_{ds})$ inferred by the eq. (2), and calculates the desired angles and angular velocities of the trajectory type by using eqs. (3)-(8).

be used to standardize the trajectory corresponding to the walking velocity. The estimated equation $V_{est}(t_{ds})$ m/s, with the proposed swing speed profile shown in Fig. 4b, is given as follows:

$$V_{est}(t_{ds}) = \begin{cases} 0.405 - 0.908\log(t_{ds}) & (0.0 < t_{ds} \leq 2.1) \\ \gamma \ \ (=const) & (t_{ds} > 2.1) \end{cases} \quad (2)$$

where γ is the constant value (=0.112), and t_{ds} s is the duration of the double stance phase until the inequalities (1) are satisfied. The calculation of each desired trajectory compatible with the swing speed profile is explained in the next subsection.

B. Desired-trajectory calculator

The desired-trajectory calculator provides the reference angle and angular velocity of each joint corresponding to the walking velocity inferred by eq. (2). Although the calculation of inverse kinematics for a multi-jointed manipulator is generally solved to smoothly connect a start-point to an end-point, an infinite number of possible trajectories exist when the inverse kinematics are calculated. In contrast, a reaching movement between two points of a healthy participant's end-effector becomes a unique trajectory with a bell-shaped velocity profile and a bimodal acceleration profile. This trajectory can be reproduced by a minimum jerk model that applies the initial and final states as boundary conditions. Therefore, this study calculates the desired trajectory using quintic spline interpolation on the basis of a minimum jerk trajectory to generate a trajectory with the characteristics mentioned above. The calculation of the desired minimum jerk trajectories makes it possible to easily calculate the desired trajectory with a bell-shaped velocity curve using geometry information, because there is no need to consider the dynamics characteristics of each link. The desired minimum jerk trajectories of the angle $\theta_{ri}(t)$ and angular velocity $\dot{\theta}_{ri}(t)$ during the swing phase are given as follows:

$$\theta_{ri}(t) = \begin{cases} \alpha_{ri}(t) & (t_a \leq t \leq t_{bi}) \\ \beta_{ri}(t) & (t_{bi} < t \leq t_c) \end{cases} \quad (3)$$

$$\dot{\theta}_{ri}(t) = \begin{cases} \dot{\alpha}_{ri}(t) & (t_a \leq t \leq t_{bi}) \\ \dot{\beta}_{ri}(t) & (t_{bi} < t \leq t_c) \end{cases} \quad (i = 1, 2, 3) \quad (4)$$

where $\alpha_{ri}(t)$ and $\beta_{ri}(t)$ are the desired trajectories of each angle for flexion and extension. $\dot{\alpha}_{ri}(t)$ and $\dot{\beta}_{ri}(t)$ are the desired trajectories of each angular velocity for flexion and extension. t_a, t_{bi}, and t_c are the time of the initial, relay, and end points. The numerical values 1, 2, and 3 denote the hip, knee, and ankle joints, respectively. These values are substituted for the 'i' of the subscript. $\alpha_{ri}(t)$, $\beta_{ri}(t)$, $\dot{\alpha}_{ri}(t)$, and $\dot{\beta}_{ri}(t)$ are calculated by:

$$\alpha_{ri}(t) = \varphi_{ai}(t_a) + (15t_j^4 - 6t_j^5 - 10t_j^3)(\varphi_{ai}(t_a) - \varphi_{bi}(t_{bi})), \quad (5)$$

$$\beta_{ri}(t) = \varphi_{bi}(t_{bi}) + (15t_k^4 - 6t_k^5 - 10t_k^3)(\varphi_{bi}(t_{bi}) - \varphi_{ci}(t_c)), \quad (6)$$

$$\dot{\alpha}_{ri}(t) = 30(2t_j^3 - t_j^4 - t_j^2)(\varphi_{ai}(t_a) - \varphi_{bi}(t_{bi})), \quad (7)$$

$$\dot{\beta}_{ri}(t) = 30(2t_k^3 - t_k^4 - t_k^2)(\varphi_{bi}(t_{bi}) - \varphi_{ci}(t_c)), \quad (8)$$

$$t_j = \frac{t - t_a}{t_{bi} - t_a} \ \text{ and } \ t_k = \frac{t - t_{bi}}{t_c - t_{bi}}, \qquad (i, j, k = 1, 2, 3)$$

where $\varphi_{ai}(t_a)$ is the initial angle of each joint when the inequalities (1) are satisfied. $\varphi_{bi}(t_{bi})$ and $\varphi_{ci}(t_c)$ are the maximum flexion and maximum extension angles during walking. The numerical values 1, 2, and 3 are substituted for the 'i,' 'j,' and 'k' of the subscript. The parameters required for the trajectory calculation, e.g., $\varphi_{bi}(t_{bi})$, $\varphi_{ci}(t_c)$, t_{bi}, and t_c, are obtained from the gait analysis of a healthy participant.

Meanwhile, the speed of the swing leg proved to be classified with four general groups according to the belt-speed of a treadmill between 0.4 km/h and 2.0 km/h from the results

This article has been accepted for publication in a future issue of this journal, but has not been fully edited. Content may change prior to final publication. Citation information: DOI 10.1109/TNSRE.2014.2364618, IEEE Transactions on Neural Systems and Rehabilitation Engineering

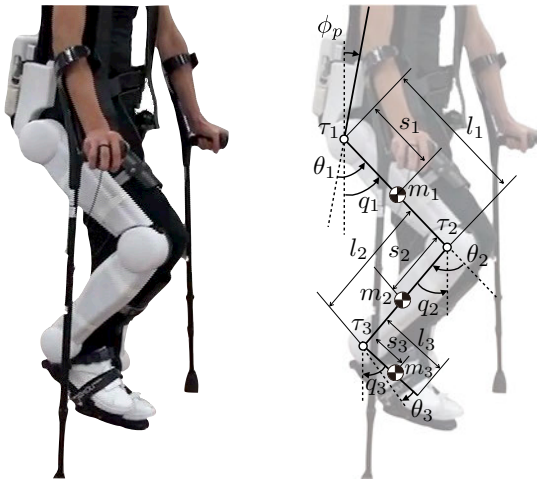

Fig. 6. Definition of dynamics parameters. The values m_*, l_*, and s_* are the mass of the link, the link length, and the position of the mass, respectively. The subscripts of the parameters 1, 2, and 3 indicate the thigh, the shank, and the foot, respectively. The values ϕ_p, θ_1, θ_2, and θ_3 are the relative angles of the upper body, hip, knee, and ankle around the pitch axis. The flexion of each joint angle is set as the positive direction. The values q_1, q_2, and q_3 are the absolute angles of the hip, knee, and ankle.

of gait analysis of healthy participant. Therefore, the desired trajectories of the angle and angular velocity that are calculated from eqs. (3)-(8) fall into four types based on the proposed swing speed profile as shown in Fig. 5.

C. Controller for gait support

In general, proportional and derivative (PD) control is widely used so that the joint angle may follow a desired trajectory that changes over time. However, feedback control methods like PD control have consistent margins of error because they calculate the command torque on the basis of the error generated from a reference. As a result, the controller causes a vibration and an overshoot as the PD gains increase to minimize the error. Therefore, to improve the response of the velocity control system without overshooting, HAL controls each actuator with combinations of PD and inverse dynamics control. The control law is calculated by:

$$\vec{\tau}(t) = \vec{K}_p \vec{e}(t) + \vec{K}_d \dot{\vec{e}}(t) + \vec{\tau}_{ff}(t), \tag{9}$$

$$\vec{\tau} = \left[\tau_1, \tau_2, \tau_3\right]^{\mathrm{T}}_{,} \quad \vec{\tau}_{ff} = \left[\tau_{ff1}, \tau_{ff2}, \tau_{ff3}\right]^{\mathrm{T}}_{,}$$
$$\vec{K}_p = \left[K_{p1}, K_{p2}, K_{p3}\right]^{\mathrm{T}}_{,} \text{ and } \vec{K}_d = \left[K_{d1}, K_{d2}, K_{d3}\right]^{\mathrm{T}}_{,}$$

where $\vec{\tau}(t)$ is the command torque of each joint, and $\vec{K}_p$ and $\vec{K}_d$ are the PD gains, respectively. The single-column matrices $\vec{e}(t) = \vec{\theta}_r(t) - \vec{\theta}(t)$ and $\dot{\vec{e}}(t) = \dot{\vec{\theta}}_r(t) - \dot{\vec{\theta}}(t)$ represent the displacement errors of the angle and angular velocity, respectively. $\vec{\tau}_{ff}(t)$ is the feedforward torque of each joint calculated by the dynamics model shown in Fig. 6 as follows:

$$\vec{\tau}_{ff}(t) = \vec{M}(\vec{q_r})\ddot{\vec{q}}_r + \vec{V}(\vec{q_r}, \dot{\vec{q}}_r) + \vec{G}(\vec{q_r}), \tag{10}$$

$$\vec{q_r} = \left[q_{r1}, q_{r2}, q_{r3}\right]^{\mathrm{T}}_{,} \quad \dot{\vec{q}}_r = \left[\dot{q}_{r1}, \dot{q}_{r2}, \dot{q}_{r3}\right]^{\mathrm{T}}_{,} \text{ and } \ddot{\vec{q}} = \left[\ddot{q}_{r1}, \ddot{q}_{r2}, \ddot{q}_{r3}\right]^{\mathrm{T}}_{,}$$

where $\vec{M}(\vec{q_r})$, $\vec{V}(\vec{q_r}, \dot{\vec{q}}_r)$, and $\vec{G}(\vec{q_r})$ are the inertial, nonlinear, and gravity terms. The single-column matrices $\vec{q_r}$, $\dot{\vec{q}}_r$, and $\ddot{\vec{q}}_r$ are the reference of the absolute angle, angular velocity, and angular acceleration, respectively. These desired trajectories are also calculated on the basis of the quintic spline interpolation in common with the calculation of the trajectories for the PD control. The elements of these matrices are described as follows:

$$\vec{M}(\vec{q_r}) = \begin{bmatrix} m_1 s_1^2 + m_2 l_1^2 + m_3 l_1^2 & (m_2 l_1 s_2 + m_3 l_1 l_2) C_{12} & m_3 l_1 s_3 C_{12} \\ (m_2 l_1 s_2 + m_3 l_1 l_2) C_{12} & m_2 s_2^2 + m_3 l_2^2 & m_3 l_2 s_3 C_{23} \\ m_3 l_1 s_3 C_{13} & m_3 l_2 s_3 C_{23} & m_3 s_3^2 \end{bmatrix}_{,} \tag{11}$$

$$\vec{V}(\vec{q_r}, \dot{\vec{q}}_r) = \begin{bmatrix} 0 & m_3 l_1 l_2 S_{12} & m_3 l_1 s_3 S_{13} \\ -(m_2 l_1 s_2 + m_3 l_1 l_2) S_{12} & 0 & m_3 l_2 s_3 S_{23} \\ -m_3 l_1 s_3 S_{13} & -m_3 l_2 s_3 S_{23} & 0 \end{bmatrix}_{,} \text{ and} \tag{12}$$

$$\vec{G}(\vec{q_r}) = \begin{bmatrix} m_1 s_1 g \sin q_{r1} + m_2 l_1 g \sin q_{r1} + m_3 l_1 g \sin q_{r1} \\ m_2 s_2 g \sin q_{r2} + m_3 l_2 g \sin q_{r2} \\ m_3 s_3 g \sin q_{r3} \end{bmatrix}_{,} \tag{13}$$

where the standard acceleration of gravity g is defined as $9.80665\ \mathrm{m/s^2}$. C_{12}, C_{23}, C_{13}, S_{12}, S_{23}, and S_{13} are defined as follows:

$$C_{12} = \cos(q_{r1} - q_{r2}),\ C_{23} = \cos(q_{r2} - q_{r3}),\ C_{13} = \cos(q_{r1} - q_{r3}), \tag{14}$$
$$S_{12} = \sin(q_{r1} - q_{r2}),\ S_{23} = \sin(q_{r2} - q_{r3}),\ \text{and}\ S_{13} = \sin(q_{r1} - q_{r3}).$$

III. Preliminary Experiments

From viewpoint of safety, the operation verification of the proposed gait support algorithms (*Gait intention estimator A and B, Desired-trajectory calculator,* and *Controller*) was implemented through two categories of preliminary experiments before the realistic tests of a SCI patient. These experiments were performed on a mannequin in place of an actual patient. The first experiment verified that HAL with the proposed algorithms allowed the mannequin to walk properly and safely. Specifically, in the second experiment, we confirmed the differences in gait characteristics caused by the presence or absence of the proposed swing speed profile (*Gait intention estimator B*).

A. Experimental setup and Procedures

The setup for the first experiment is shown in Fig. 7. HAL with the proposed algorithms (*Gait intention estimator A and B, Desired-trajectory calculator,* and *Controller*) makes a mannequin walk on the ground. The mannequin simulates the physical conditions of a SCI patient who has completely impaired lower limb motor and sensory functions. The total weight of the mannequin is approximately 75 kg. The mannequin equipped with HAL is connected to a wheeled unweighting device by a sling belt. Since the mannequin cannot take an action related to the swing leg by itself, an experimenter pushes the device forward to shift the weight of the mannequin.

In the second experiment, the GRF distribution and the upper body angle are measured when the system with/without the swing speed profile (*Gait intention estimator B*) supports the mannequin's walk on a treadmill using an unweighting device. Note, however, that the other algorithms (*Gait intention*

This article has been accepted for publication in a future issue of this journal, but has not been fully edited. Content may change prior to final publication. Citation information: DOI 10.1109/TNSRE.2014.2364618, IEEE Transactions on Neural Systems and Rehabilitation Engineering

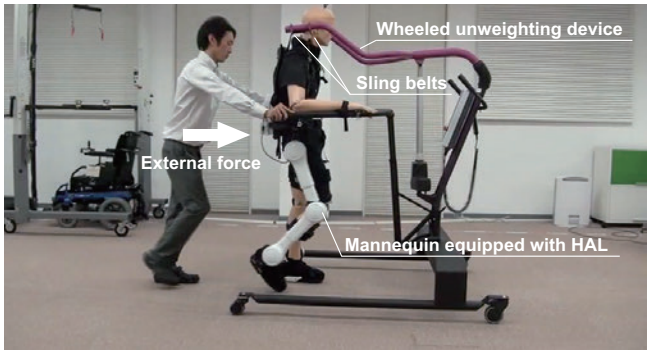

Fig. 7. Experimental setup for the preliminary experiments. An external force caused by pushing the wheeled unweighting device produces the weight shift of the mannequin equipped with HAL.

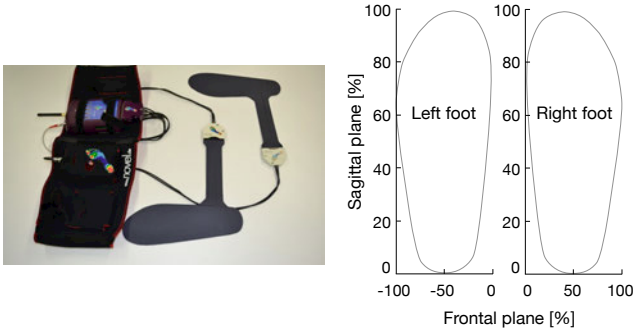

(a) (b)

Fig. 8. (a) The pedar-x system (Novel Electronics Inc.). (b) The coordinate axes of each leg in the sagittal and frontal planes.

estimator A, Desired-trajectory calculator, and *Controller*) are built into HAL regardless of the presence or absence of the swing speed profile. The treadmill speed is changed between 0.4 km/h to 2.0 km/h at random. The GRF distribution is measured at 100 Hz using an in-shoe pressure distribution measuring system shown in Fig. 8a. The sensing parts of the system compose 99-part capacitive pressure sensors at each foot. Therefore, the system also measures the CoGRF in real time. The origin coordinate of each leg is located at the medial lower corner of the insole shape as shown in Fig. 8b.

B. Results

1) First preliminary experiment: Figure 9 shows the results of the first preliminary experiment using the mannequin equipped with HAL including the proposed algorithms. HAL started the swing phase alternately when the inequalities (1) were satisfied by the external force during the double stance phase. At the same time, the walking velocity was successfully inferred by assigning the duration of the double stance phase to eq. (2), and thereby the desired trajectory of each joint corresponding to the inferred walking velocity was calculated using eqs. (3)-(8). From these results, each link rotated in synchronization with the other links using the control law expressed in eq. (9).

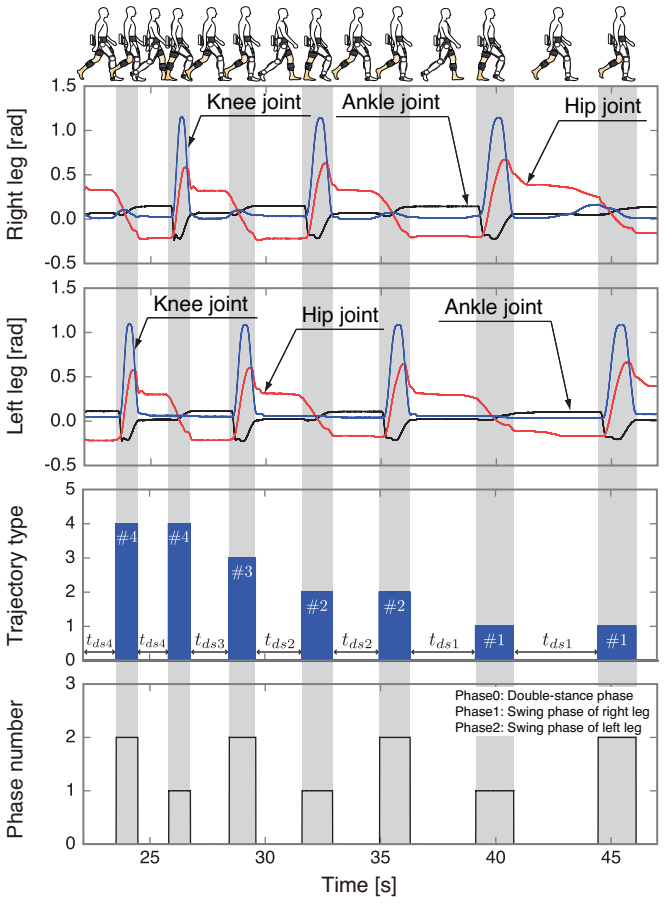

Fig. 9. Result of the first preliminary experiment. These graphs show the displacement of each joint angle, the desired trajectory type, and the phase number. The walking velocity was inferred by substituting the duration of the double stance phase (t_{ds1}, t_{ds2}, t_{ds3},, and t_{ds4}) into eq. (2), while the conditions described in the inequalities (1) were satisfied. Then, the reference of the trajectory type corresponding to the estimated walking velocity were calculated using eq. (3)-(8). As a result, HAL started the swinging support using eq. (9) while adjusting the walking velocity.

2) Second preliminary experiment: The gait support system, with or without the proposed swing speed profile, allowed the mannequin to walk on a treadmill. However, when the treadmill speed was randomly changed, there were critical differences in the GRF distribution and the upper body angle around the pitch axis as shown in Figs. 10 and 11. The gait support algorithms with the swing speed profile successfully changed the speed of the swing leg according to the treadmill speed, so that the floor contact occurred at the heel part (rearfoot strike: RFS) immediately before forefoot came down. As a result, the GRF was evenly distributed on the regions from the rearfoot to the forefoot as shown in Fig. 10a. In contrast, the walking velocity using the algorithms without the swing speed profile was sometimes slower than the treadmill speed, and so the floor contact occurred at the toe part (forefoot strike: FFS). For this reason, the GRF was distributed to the forefoot regions as shown in Fig. 10b. The differences in landings affected the upper body angle around the pitch axis ϕ_p shown in Fig. 11. The landing pattern of the RFS generated by the algorithms with the swing speed profile maintained

This article has been accepted for publication in a future issue of this journal, but has not been fully edited. Content may change prior to final publication. Citation information: DOI 10.1109/TNSRE.2014.2364618, IEEE Transactions on Neural Systems and Rehabilitation Engineering

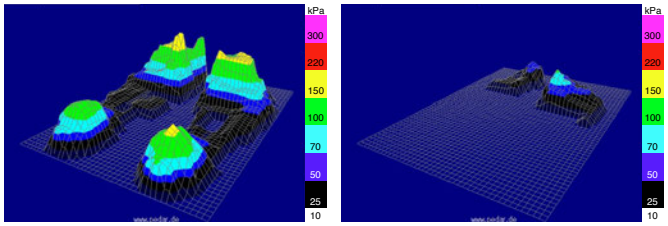

(a) Variable swing speed (b) Constant swing speed

Fig. 10. The GRF distribution when the trajectory of the swing leg was adjusted using the gait intention estimator with the proposed swing speed profile (a), when the trajectory was constant using the estimator without the swing speed profile (b).

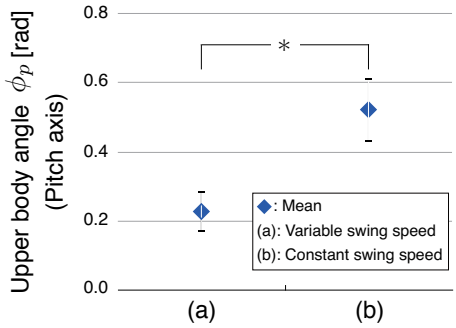

Fig. 11. The upper body angle around the pitch axis with or without the swing speed profile. Error bars represent standard deviation (SD). The results of the t-test are shown in this figure as '*' for p-values$<$0.001 to demonstrate the statistical significance of the proposed swing speed profile.

the upper body angle at 0.228$\pm$0.058 rad, whereas the FFS generated by the algorithms without the profile inclined the angle at 0.522$\pm$0.094 rad owing to the delay of the swing leg. There was a statistically significant difference ($p<0.001$) between them. The probability value (p-value) was calculated using a Student's paired t-test.

Consequently, we verified that the mannequin's walk was controlled properly and safely with the proposed gait support algorithms in the first preliminary experiments. In particular, the effectiveness of the proposed swing speed profile was confirmed through the second experiment.

IV. Realistic tests

To demonstrate the practical feasibility of HAL with the proposed algorithms, we conducted realistic tests with a SCI patient wearing the gait support system for six days during a period of 3 months. The realistic tests were performed in accordance with procedures approved by the Institutional Review Board. The patient participated in the tests after giving their informed consent.

A. Participant

The target patients for the gait support system are SCI patients who have impaired lower limb motor and sensory functions with sufficient physical ability in their upper limbs to convey the intention related to the swing leg to the system by shifting their body weight. For this reason, we selected a 39-year-old man who had spinal cord damage at Th7 and Th8 due to a traffic accident (ASIA classification; grade A). The patient underwent gait training with the lower limb orthosis and Lofstrand crutches under the supervision of physical therapists after receiving olfactory mucosa autografts into their injured spinal cord in 2010 [22]. The rank of the walking capability corresponded to level 12 of the Walking Index for Spinal Cord Injury Version 2 (WISCI-II) [23]–[25].

B. Experimental evaluations and Procedures

The walking capability of the patient supported by the gait support system was quantitatively evaluated using the following indices throughout the realistic tests.

- 10MWT
- Symmetric property

The 10MWT measures the walking time, the number of steps, and the cadence required to walk 10 meters [26]. The patient wearing the system used two forearm crutches to shift the own body weight and to keep the balance during the 10MWT. Also, HAL was connected to a movable ceiling suspension device with a sling belt to eliminate the risk of unexpected falling. However, the device was normally slack so as not to disturb the gait of the patient. The symmetric property is assessed based on the CoGRF distribution between the right and left legs and the double stance time at the left-forefoot and right-forefoot. The symmetry of the CoGRF distribution is calculated by:

$$SP_* = \frac{\overline{A}_* - \overline{B}_*}{\overline{A}_* + \overline{B}_*} \tag{15}$$

where $\overline{A}_*$ and $\overline{B}_*$ are the mean distributions of the CoGRF at the right and left legs, respectively. The asterisk of the subscript denotes the anterior-posterior (AP) or medial-lateral (ML) directions. When the walking motion becomes more bilaterally symmetric from a spatial viewpoint, SP_{AP} and SP_{ML} approach zero. The symmetry of the double stance time is also calculated by:

$$SP_{DS} = \frac{\overline{DS}_1 - \overline{DS}_2}{\overline{DS}_1 + \overline{DS}_2} \tag{16}$$

where $\overline{DS}_1$ and $\overline{DS}_2$ are the mean times of the double stance phase at the left-forefoot and right-forefoot, respectively. When the walking motion becomes more bilaterally symmetric and the gait becomes more rhythmic from a temporal viewpoint, SP_{DS} approaches zero.

In the final day of the tests, the patient conducted the 10MWT using the gait support system or a knee-ankle-foot orthosis (KAFO) to compare the difference in gait quality between the two types.

C. Results

1) 10MWT: The sequential photographs shown in Fig. 12 depict the 10-meter walk of the SCI patient using two forearm crutches and HAL with the proposed algorithms. After the IC phase, the system estimated the wearer's intention to swing

This article has been accepted for publication in a future issue of this journal, but has not been fully edited. Content may change prior to final publication. Citation information: DOI 10.1109/TNSRE.2014.2364618, IEEE Transactions on Neural Systems and Rehabilitation Engineering

(a) IC (b) LR (c) MSt (d) TSt (e) PSw (f) ISw (g) MSw (h) TSw

Fig. 12. Sequential photographs of the gait support for the SCI patient during one gait cycle in 10MWT. Each phase is defined as follows: (a) Initial contact (IC), (b) Loading response (LR), (c) Mid stance (MSt), (d) Terminal stance (TSt), (e) Pre-swing (PSw), (f) Initial swing (ISw), (g) Mid swing (MSw), and (h) Terminal swing (TSw).

TABLE I
RESULTS OF THE 10-METER WALK TEST.

	Evaluation index of 10MWT		
Days	**Walking time [s]**	**Number of steps [steps]**	**Cadence [steps/min]**
1st	80.50±2.12	35.0±1.41	26.09±0.35
2nd	80.09±8.85	36.0±1.27	26.97±1.83
3rd	62.09±4.76	33.0±2.16	31.89±0.33
4th	60.69±4.81	32.3±1.80	31.92±0.69
5th	61.28±4.08	34.0±1.00	33.29±1.16
6th	62.58±2.82	34.5±0.33	33.08±1.12

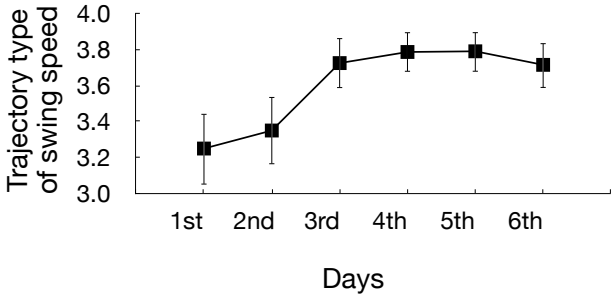

Fig. 13. The mean trajectory type of swing speed through the realistic tests. This result shows that the system supported the SCI patient's gait while adjusting the speed of the swing leg using the swing speed profile from the gait intention estimator. The speed is determined based on the duration of the double stance phase immediately before the swing phase.

the contralateral leg when the patient shifted the body weight towards the forefoot side using the forearm crutches during the LR phase. In the MSt phase and the TSt phase, the system controlled the extension of the hip joint while sustaining the wearer's body weight to support the forward movement. At the same time, the system also controlled the contralateral swing leg. After the TSt phase, the system estimated the wearer's intention related to the swing leg when the patient shifted the body weight toward the forefoot side using the forearm crutches during the PSw phase. During the ISw phase, the MSw phase, and the TSw phase, the system controlled the forward swing of the leg. Table I shows the results of walking time, number of steps, and cadence for all test days. Compared with the results for the 1st day, the results of walking time and cadence on the 6th day improved approximately 22.26% and 26.79%, respectively. Even though the number of steps did not change much throughout the tests, the trajectory type of swing speed shown in Fig. 13 was successfully adjusted by the swing speed profile.

2) Symmetric property: From a spatial viewpoint, the mean distributions of the CoGRF between the right and left legs were almost symmetrical in the sagittal and frontal planes as shown in Fig. 14. Figure 15 shows the symmetric index of the double stance time between the DS_1 and the DS_2 from a temporal viewpoint. Although the results in the first and second days lost symmetry, the double stance time became symmetrical from the third day. At the same time, the walking speed increased as shown in Fig. 13.

3) HAL vs. KAFO: The patient achieved the 10MWT using the gait support system or the KAFO. Both results corresponded to a WISCI-II level of 12. However, the results showed critical differences in both CoGRF distribution and walking time. Figure 16a shows that the CoGRF distribution was located on the area between the posterior part and anterior part of the sole, when the patient received gait support from the system. In contrast, the CoGRF distribution shown in Fig. 16b was located on the narrow area of the anterior part of the sole when the patient walked using the KAFO. The mean walking time shown in Fig. 17 indicates that the system allowed the patient to walk 10 meters in 62.58±2.82 s whereas the patient fitted with the KAFO walked 10 meters in 79.91±5.52 s. This result also means that the walking time of the gait support system was about 21.69% shorter than that of the KAFO. There was a statistically significant difference ($p<0.001$) between them.

V. DISCUSSION

The aim of this study was to propose a novel gait intention estimator that not only detects the moment of starting a swing leg based on the CoGRF behavior but also infers the swing speed depending on the walking velocity, so that the system could perform the assistance reflecting the gait intention of a severe SCI patient at a higher level.

In the preliminary experiments, we checked that the proposed gait support algorithms (*Gait-intention estimator A and B, Desired-trajectory calculator,* and *Controller*) effectively worked as shown in Fig. 9. In particular, the results of the second experiment verified the effectiveness of the gait

This article has been accepted for publication in a future issue of this journal, but has not been fully edited. Content may change prior to final publication. Citation information: DOI 10.1109/TNSRE.2014.2364618, IEEE Transactions on Neural Systems and Rehabilitation Engineering

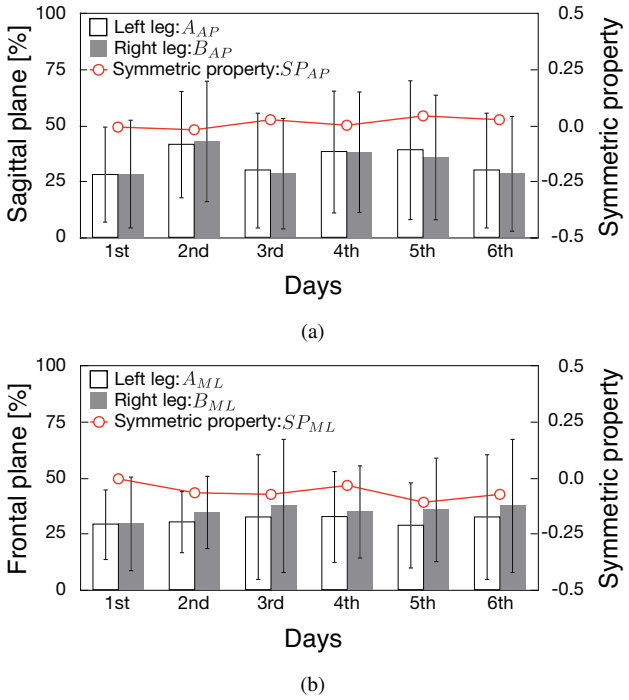

Fig. 14. The polygonal lines in these bar graphs indicate the spatial symmetry between the right and left legs in the sagittal (a) and frontal (b) planes during the gait support of the system. The gray and white bars show the CoGRF distribution of the right and left legs, respectively.

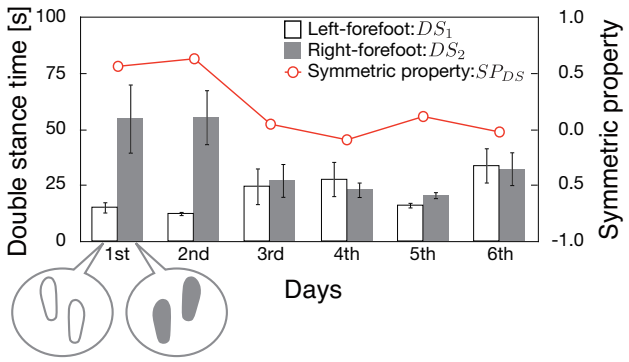

Fig. 15. The polygonal lines in these bar graphs indicate the temporal symmetry between the right and left legs during the gait support of the system. The gray and white bars show the double stance time of the right-forefoot and left-forefoot, respectively.

intention estimator including the swing speed profile. In the gait support system with the proposed swing speed profile, the GRF shown in Fig. 10a was distributed over the entire region of the sole while upper body angle around the pitch axis shown in Fig. 11a maintained a nearly upright posture, because the swing speed corresponded to the random variation of the treadmill speed. In contrast, the GRF shown in Fig. 10b was distributed to the foreside of the sole while the upper body angle shown in Fig. 11b inclined forward by the gait support of the system without the swing speed profile, because the swing speed was slower than the treadmill speed. In previous studies, the smooth transition of the CoGRF is accomplished by rocker functions that describe the rotational motion of the

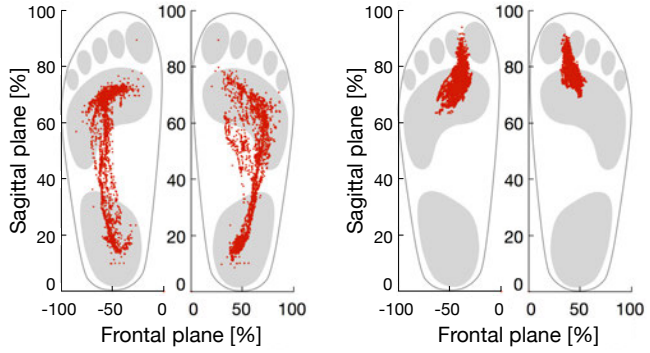

Fig. 16. The CoGRF distribution (a) when HAL with the proposed algorithms was used, (b) when a KAFO was used during the 10MWT.

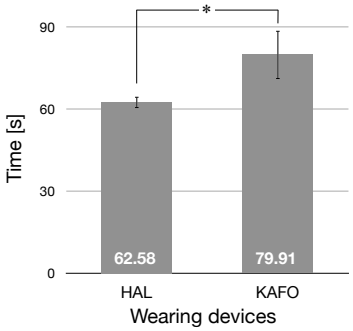

Fig. 17. The walking time of the gait support system versus a KAFO. When the system supported the patient's gait, the walking time was shortened 21.69% compared with when the patient was fitted with a KAFO. The t-test results are shown in this figure as '*' for p-values$<$0.001 to demontsrate the statistical significance of the gait support system.

stance leg from the RFS in the IC to the heel-off in the TSt [27]–[29]. The rocker functions not only generate the forward-momentum necessary to increase the walking velocity, but also prevent the upper body angle around the pitch axis from bending excessively [30]. In other words, when the forepart of the foot touches the ground at the moment of IC, it is difficult to walk and maintain upright posture owing to the FFS produced by the loss of the heel rocker function. The loss of the heel rocker also causes a decrease in walking velocity. On the basis of these results and the kinematics of human gait, we indicate that the gait support system with the proposed swing speed profile allows the mannequin to walk properly and safely at various treadmill speeds.

In the realistic tests, we demonstrated the practical feasibility of HAL with the proposed algorithms by providing gait support to the SCI patient. As shown in Table I, the cadence and walking time of the 10MWT were gradually improved throughout the realistic tests. These results are attributed to the fact that the system increased the speed of the swing leg using the swing speed profile (see Fig. 13). From the spatial perspective, the symmetric properties of the CoGRF distribution between the right and left legs were evaluated quantitatively as shown in Fig. 14. The CoGRF distribution

became mostly symmetric in the sagittal and frontal planes. This result indicates that the symmetrical CoGRF distribution between the right and left legs ensured a balance during HAL's gait support. Figure 15 evaluated the symmetrical gait between the right and left legs from the temporal perspective. The double stance time between the left-forefoot and the right-forefoot was asymmetrical in the first and second tests, because the system started the swing phase when the inequalities (1) were satisfied based on the impact of the foot landing. Although the original threshold of the hip joint angle was defined on the basis of the gait analysis of a healthy participant, we adjusted the threshold according to the physical condition of the patient's leg so as not to initiate the swing phase based on the physical impact. As a result, the system allowed the wearer to produce symmetrical and rhythmical gait from the 3rd test. Both the gait support provided by the system and the use of a KAFO enabled the patient to walk 10 meters as shown on the final day's results. The evaluation indices, e.g., the WISCI-II or the Spinal Cord Independence Measure (SCIM), do not take the outcome of the CoGRF and 10MWT into account to categorize the level of a SCI patient's gait capability. It is therefore difficult to use them to assess a SCI patient's gait quantitatively [23]–[26]. However, crucial differences were found in the CoGRF distribution and the walking time as shown in Figs. 16 and 17. The patient wearing the KAFO lifted the leg using the upper limbs and a twist of the upper body, and then swung the leg forward like a pendulum. Since the muscle contraction required for a heel strike is not triggered by the loss of lower limb motor and sensory functions, the patient could not control the landing position of the foot. The patient therefore repeated the gait in the FFS pattern that is not observed in natural gait. Conversely, the gait support system controlled the coordinated motion of each joint depending on the inferred walking velocity while bearing the wearer's weight. For this reason, the patient produced a gait in the FFS pattern that is attributable to the generation of the rocker functions required for increasing the walking velocity.

The advantage of our system is that "the gait intention estimator" infers the swing speed as well as detects the moment to start the swing leg based on the CoGRF behavior instead of detecting BES. The target patient therefore requires the physical ability that intentionally generates the sway of the body trunk using a walking aid to convey the gait intention to the proposed estimator. Most severe SCI patients cannot intentionally generate the BES from their lower limbs because of injury to their central nervous system. Even if the patients undergo spinal cord stem cell transplants, it is difficult to detect the appropriate BES. Therefore, our study has clinical importance as an early-stage gait support.

The limitations of this study include that the number of participant is small. In the next stage, we are currently performing the clinical trials with more SCI patients for regular and long periods to evaluate the usability of the gait support system and to observe the degree of functional recovery in the lower limbs. Besides, we are developing a hybrid method that combines the system used in this study with the voluntary control method based on the BES [6], [7] for the SCI patients who expect the recovery of motor and sensory functions.

VI. Conclusions

The paper proposed a novel gait intention estimator that not only detects the moment to start a swing leg based on the CoGRF behavior but also infers the swing speed based on the walking velocity, so that the system could provide the assistance synchronized with the gait intention of a severe SCI patient at a higher level. First, we revealed the relationship between the speed of the swing leg and the duration of the double stance phase by the gait analysis, and then developed the gait support algorithms. Second, preliminary experiments for the gait support were conducted using a mannequin equipped with HAL including the proposed algorithms. Finally, realistic tests consisting of a 10MWT were conducted on a severe SCI patient wearing the gait support system. The results of the tests showed that the system supported the patient's gait while adjusting the speed of the swing leg. Furthermore, the crucial differences of gait between the system and the KAFO were found in the CoGRF distribution and the walking time. In consequence, we demonstrated the effectiveness and practical feasibility of the proposed gait support algorithms.

Acknowledgements

This study was supported by the "Center for Cybernics Research (CCR) - World Leading Human-Assistive Technology Supporting a Long-Lived and Healthy Society" granted the "Funding Program for World-Leading Innovative R&D on Science and Technology (FIRST Program)," initiated by the Council for Science and Technology Policy (CSTP) and JSPS KAKENHI Grant Number 23700660.

References

[1] S. Goemaere M. Van Laere, P. De Neve, and J. M. Kaufman, Bone Mineral Status in Paraplegic Patients Who Do or Do Not Perform Standing, *Osteoporosis International*, vol. 4, pp. 138-143, 1994.

[2] R.W. Teasell, T.J. Hsieh, JA. L. Aubut, J.J. Eng, A. Krassioukov, L. Tu, and the SCIRE Research Team, Venous Thromboembolism After Spinal Cord Injury, *Archives of Physical Medicine and Rehabilitation*, vol. 90, pp. 232-245, 2009.

[3] G. Arpaiaa, P.M. Baverab, D. Caputoc, L. Mendozzic, R. Cavarrettac, G.B. Agusd, M. Milania, E. Ippolitod, and C. Cimminiellоa, Risk of deep venous thrombosis (DVT) in bedridden or wheelchair-bound multiple sclerosis patients: A prospective study, *Thrombosis Research*, vol. 125, pp. 315-317, 2010.

[4] Kenneth T. Horlander, David M. Mannino, and Kenneth V. Leeper, Pulmonary Embolism Mortality in the United States, 1979-1998: An Analysis Using Multiple-Cause Mortality Data, *Archives of Internal Medicine*, vol. 163, pp. 1711-1717, 2003.

[5] I.A. Næss, S.C. Christiansen, P. Romundstand, S.C. Cannegieter, and F.R. Rosendaal, Incidence and mortality of venous thrombosis, *J. of Thrombosis and Haemostasis*, vol. 5, pp. 692-699, 2007.

[6] S. Lee and Y. Sankai, Power assist control for walking aid with HAL-3 based on EMG and impedance adjustment around knee joint, in *Proc. of the 2002 IEEE/RSJ Int'l Conf. on Intelligent Robots and Systems (IROS 2002)*, Lausanne, Switzerland, pp. 1499-1504, 2002.

[7] T. Hayashi, H. Kawamoto, and Y. Sankai, Control Method of Robot Suit HAL working as Operator's Muscle using Biological and Dynamical Information, *Proc. of the 2005 IEEE/RSJ Int'l Conf. on Intelligent Robots and Systems (IROS 2005)*, pp. 3063-3468, 2005.

[8] H. Kawamoto and Y. Sankai, Power Assist Method Based on Phase Sequence and Muscle Force Condition for HAL, *Advanced Robotics*, vol. 19, pp. 717-734, 2005.

[9] K. Suzuki, G. Mito, H. Kawamoto, Y. Hasegawa, and Y. Sankai, Intention-Based Walking Support for Paraplegia Patients with Robot Suit HAL, *Advanced Robotics*, vol. 21, pp. 1441-1469, 2007.

[10] A. Tsukahara, R. Kawanishi, Y. Hasegawa, and Y. Sankai, Sit-To-Stand and Stand-To-Sit Transfer Support for Complete Paraplegic Patients with Robot Suit HAL, *Advanced Robotics*, vol. 24, pp. 1615-1638, 2010.

[11] A. Tsukahara, Y. Hasegawa, and Y. Sankai, Gait Support for Complete Spinal Cord Injury Patient by Synchronized Leg-Swing with HAL, *Proc. of the 2011 IEEE/RSJ Int'l Conf. on Intelligent Robots and Systems (IROS2011)*, pp. 1737-1742, 2011.

[12] R.J. Farris, H.A. Quintero, and M. Goldfarb, Preliminary Evaluation of a Powered Lower Limb Orthosis to Aid Walking in Paraplegic Individuals, *IEEE Trans. Neural Syst Rehab Eng*, vol. 19, pp. 652-659, 2011.

[13] M. Talaty, A. Esquenazi, and J.E. Briceno, Differentiating Ability in Users of the ReWalk Powered Exoskeleton: An Analysis of Walking Kinematics, *Proc. of the 2013 IEEE Int'l Conf. on Rehabilitation Robotics (ICORR 2013)*, pp. 24-26, 2013.

[14] K.A. Strausser and H. Kazerooni, The Development and Testing of a Human Machine Interface for a Mobile Medical Exoskeleton, *Proc. of the 2011 IEEE/RSJ Int'l Conf. on Intelligent Robots and Systems (IROS2011)*, pp. 4911-4916, 2011.

[15] T. Kagawa and Y. Uno, A human interface for stride control on a wearable robot, *Proc. of the 2009 IEEE/RSJ Int'l Conf. on Intelligent Robots and Systems (IROS 2009)*, pp. 4067-4072, 2009.

[16] S. Tanabe, S. Hirano, and E. Saitoh, Wearable Power-Assist Locomotor (WPAL) for supporting upright walking in persons with paraplegia, *NeuroRehabilitation*, vol. 33, pp. 99-106, 2013.

[17] P. Rossier and D.T. Wade, Validity and Reliability Comparison of 4 Mobility Measures in Patients Presenting with Neurologic Impairment, *Archives of Physical Medicine and Rehabilitation*, vol. 82, pp. 9-13, 2001.

[18] H.J. van Hedel, M. Wirz, and V. Dietz, Assessing walking ability in subjects with spinal cord injury: validity and reliability of 3 walking tests, *Archives of Physical Medicine and Rehabilitation*, vol. 86, pp. 190-196, 2005.

[19] H.J. van Hedel, V. Dietz, and A. Curt, Assessment of walking speed and distance in subjects with an incomplete spinal cord injury, *Neurorehabilitation and Neural Repair*, vol. 21, pp. 295-301, 2007.

[20] M.P. Murray, A.B. Drought, and R.C. Kory, Walking Patterns of Normal Men, *J. Bone Joint Surg Am*, vol.46, pp.335-360, 1964.

[21] T.P. Andriacchi, J.A. Ogle, and J.O. Galante, Walking speed as a basis for normal and abnormal gait measurements, *J. Biomechanics*, vol. 10, pp. 261-268, 1977.

[22] C. Lima, P. Escada, J. Pratas-Vital, C. Branco, CA. Arcangeli, G. Lazzeri, C. Alberto Santana Maia, C, Capucho, A. Hasse-Ferreira, and J.D. Peduzzi, Olfactory Mucosal Autografts and Rehabilitation for Chronic Traumatic Spinal Cord Injury, *Neurorehabil Neural Repair*, vol. 24, pp. 10-22, 2010.

[23] B. Morganti, G. Scivoletto, P. Ditunno, JF. Ditunno, and M. Molinari, Walking index for spinal cord injury (WISCI): criterion validation, *Spinal Cord*, vol. 43, pp. 27-33, 2005.

[24] J.F. Ditunno, G. Scivoletto, M. Patrick, F. Biering-Sorensen, R. Abel, and R. Marino, Validation of the walking index for spinal cord injury in a US and European clinical population, *Spinal Cord*, vol. 46, pp. 181-188, 2008.

[25] RJ. Marino, G. Scivoletto, M. Patrick, F. Tamburella, MS. Read, AS. Burns, W. Hauck, and J. Ditunno, Walking index for spinal cord injury version 2 (WISCI-II) with repeatability of the 10-m walk time: Inter- and intrarater reliabilities, *Physical Medicine & Rehabilitation*, vol. 89, pp. 7-15, 2010.

[26] H.J.A. van Hedel, M. Wirz, and V. Dietz, Standardized assessment of walking capacity after spinal cord injury: the European network approach, *Neurological Research*, vol. 30, pp. 61-73, 2008.

[27] T.R. Han, N.J. Paik, and MS. Im, Quantification of the path of center of pressure (COP) using an F-scan in-shoe transducer, *Gait & Posture*, vol. 10, pp. 248-254, 1999.

[28] MC. Chiu, HC. Wu, and LY. Chang, Gait speed and gender effects on center of pressure progression during normal walking, *Gait & Posture*, vol. 37, pp. 43-38, 2013.

[29] MC. Chiu, HC. Wu, LY. Chang, and MH. Wu, Center of pressure progression characteristics under the plantar region for elderly adults, *Gait & Posture*, vol. 37, pp. 408-412, 2013.

[30] K.J. Nolan and M. Yarossi, Preservation of the first rocker is related to increases in gait speed in individuals with hemiplegia and AFO, *Clinical Biomechanics*, vol. 26, pp. 655-660, 2011.

Atsushi Tsukahara received the B.E. degree from Nihon University, the M.E., and Ph.D. degrees in engineering from University of Tsukuba, Japan in 2005, 2007, and 2010, respectively.

He is currently a Post Doctoral Researcher of the Center for Cybernics Research (CCR), University of Tsukuba. His research interests include assistive system for physically challenged persons, biomedical engineering, and rehabilitation robotics. He is a member of the IEEE and the Robotics Society of Japan (RSJ).

Yasuhisa Hasegawa received the B.E., and M.E. degrees from Nagoya University, Japan in 1994 and 1996, respectively. From 1996 to 1998, he worked for Mitsubishi Heavy Industries ltd., Japan. He joined Nagoya University in 1998 as a Research Associate and received the Ph.D. degree in engineering from Nagoya University in 2001. From 2003 to 2004, he was an Assistant Professor at Gifu University, Japan. From 2004 to 2007, he was an Assistant Professor at University of Tsukuba, Japan. From 2007 to 2014, he was an Associate Professor at the Center for Cybernics Research (CCR), and also the Faculty of Engineering, Information and Systems, University of Tsukuba.

He is currently a Professor of the Department of the Micro-Nano Systems Engineering, Nagoya University. He is a member of the IEEE, Japan Society of Mechanical Engineers (JSME), the Robotics Society of Japan (RSJ), the Society of Instrument and Control Engineers (SICE), Japan Society for Fuzzy Theory and Intelligent Information (SOFT).

Kiyoshi Eguchi received the B.M., and Ph.D. degrees in medical science from University of Tsukuba, Japan in 1982 and 1993, respectively. Since 1989, He has been a board certified specialist of the Japanese Association of Rehabilitation Medicine. From 1993 to 2000, he worked as an Assistant Professor at the Department of Rehabilitation Medicine, Saitama Medical School, Japan.

He is currently an Associate Professor at the Faculty of Medicine, and also the Chief of the University Hospital's Department of Rehabilitation Medicine, University of Tsukuba. His research interests include robot assisted neurorehabilitation and comprehensive rehabilitation of the disabled.

Yoshiyuki Sankai received the Ph.D. degree in engineering from University of Tsukuba, Japan in 1987. He was Research Fellow of Japan Society for the Promotion of Science, Assistant Professor, Associate Professor, Professor at the Graduate School of Systems and Information Engineering, University of Tsukuba, and a Visiting Professor of Baylor College of Medicine in Houston, Texas.

He is currently a Professor of the Faculty of Engineering, Information and Systems, University of Tsukuba, the Director of the Center for Cybernics Research (CCR), University of Tsukuba, the President and CEO of CYBERDYNE, Inc., and the Program Manager of the Impulsing Paradigm Change through Disruptive Technologies (ImPACT) Program, initiated by the Council for Science, Technology and Innovation of the Cabinet Office, Government of Japan. He was also the Principal Investigator of the Funding Program for World-Leading Innovative R&D on Science and Technology (FIRST Program), initiated by the Council for Science and Technology Policy (CSTP) of the Cabinet Office, Government of Japan, the President of Japan Society of Embolus Detection and Treatment, and an Executive Board Member of the International Journal of the Robotics Society of Japan (RSJ).